JOURNAL OF COMPUTATIONAL PHYSICS 91, 441–459 (1990)

# Solitary Waves of the Regularised Long-Wave Equation

L. R. T. GARDNER AND G. A. GARDNER

*School of Mathematics, University of Wales, University College of North Wales, Bangor, Gwynedd, LL57 1UT, United Kingdom*

Received March 22, 1988; revised December 27, 1989

A finite element solution of the Regularised Long Wave Equation, based on Galerkin's method using cubic splines as element shape functions, is set up. A linear stability analysis shows the scheme to be unconditionally stable. Test problems, including the migration and interaction of solitary waves, are used to validate the method, which is found to be accurate and efficient. The three invariants of the motion are evaluated to determine the conservation properties of the algorithm. The temporal evolution of a Maxwellian initial pulse is then studied. © 1990 Academic Press, Inc.

## 1. INTRODUCTION

Solitary waves are wave packets or pulses which propagate in nonlinear dispersive media. Due to dynamical balance between the nonlinear and dispersive effects these waves retain a stable waveform. A soliton is a very special type of solitary wave which also keeps its waveform after collision with other solitons.

The Regularised Long Wave (RLW) Equation is an alternative description of nonlinear dispersive waves to the more usual Korteweg–de Vries (KdV) equation [1]. It has been shown to have solitary wave solutions and to govern a large number of important physical phenomena such as shallow water waves and plasma waves [1, 2].

Few analytic solutions are known. Numerical solutions based on finite difference techniques [3], Runge Kutta and predictor/corrector [4] methods, and Galerkin's method [5, 6] have been given. In an implementation of Galerkin's method, Wahlbin [6] used a trial function composed of Hermite cubic polynomials, while Alexander and Morris [5] constructed a global trial function mainly from cubic splines. In the latter case the closure at the boundaries was effected with quintic polynomials and an implicit finite element approach used, in which the element matrices were not explicitly formed, but the global trial function was used directly to determine the global equations. Alexander and Morris [5] solve the resulting system of ordinary differential equations using the IMSL Library (1975) routine DREBS. In the present paper we set up an explicit finite element solution using



0021-9991/90 $3.00



581/91/2-13

cubic $B$-splines [7] as the element "shape" and weight functions throughout the solution region. The element matrices are determined algebraically using the computer algebra package REDUCE [8]. The equations governing the problem are obtained by explicitly assembling together the element matrices to obtain the full global matrix equation. The time integration used to solve the resulting system of ordinary differential equations involves a Crank–Nicholson scheme together with an inner iteration to cope with the nonlinear term; details are given in Section 3. A linear stability analysis of the numerical scheme shows it to be unconditionally stable.

The method is shown to represent accurately the migration of a single solitary wave. The interaction of two solitary waves is then studied in detail. Finally the evolution of a Maxwellian initial condition into stable solitary waves is investigated.

## 2. The Governing Equation

The RLW equation derived for long waves propagating in the positive $x$-direction has the form [1]

$$V_t + V_x + VV_x - \delta V_{xxt} = 0,$$

where $\delta$ is a positive parameter and the subscripts $x$ and $t$ denote differentiation, with the boundary condition $V \to 0$ as $x \to \pm\infty$.

Using the mapping $U = V + 1$ we can transform this equation to

$$U_t + UU_x - \delta U_{xxt} = 0 \tag{1}$$

with boundary condition $U \to 1$ as $x \to \pm\infty$. In this paper we consider the RLW equation to be of form (1) and use periodic boundary conditions for a region $a \leqslant x \leqslant b$. The form of the initial pulse is chosen so that at large distances from the pulse the function $U$ tends to 1 to agree with the physical boundary condition.

With weight function $W(x)$ Galerkin's method produces for Eq. (1) the integral

$$\int_a^b W(U_t + UU_x - \delta U_{xxt})\, dx = 0. \tag{2}$$

The presence of the second spatial derivative in the integrand implies that the interpolation function and its first derivative must be continuous throughout the region $a \leqslant x \leqslant b$. If we integrate by parts we find that

$$\int_a^b W(U_t + UU_x)\, dx + \int_a^b \delta W_x\, U_{xt}\, dx = 0. \tag{3}$$

The requirement on the interpolation functions is now simply that only the functions themselves need be continuous throughout the region. This is a minimum requirement and we have chosen to use as "shape" and weight functions the very adaptable cubic $B$-splines with their well-known advantages.

The initial conditions on the function $U(x, t)$ are prescribed in Section 6 when the test problems are discussed.

## 3. The Finite Element Solution

Cubic $B$-splines are used to approximate the solution $U(x, t)$. Let $a = x_0 < x_1 < x_2 < \cdots < x_N = b$ be a partition of $[a, b]$ by the points $x_i$, and let $\phi_i(x)$ be cubic $B$-splines with knots at the points $x_i$. The set of splines $\{\phi_{-1}, \phi_0, ..., \phi_N, \phi_{N+1}\}$ form a basis for functions defined over $[a, b]$ [7]. We seek the approximation $U_N(x, t)$ to the solution $U(x, t)$ which uses these splines as trial functions

$$U_N(x, t) = \sum_{l=-1}^{N+1} c_l(t)\, \phi_l(x), \tag{4}$$

where the $c_l$ are time dependent quantities to be determined from Eq. (3).

We identify the finite elements with the intervals $[x_l, x_{l+1}]$ with nodes at $x_l$ and $x_{l+1}$. Each cubic $B$-spline covers four elements [7]; consequently each element $[x_l, x_{l+1}]$ is covered by four splines $(\phi_{l-1}, \phi_l, \phi_{l+1}, \phi_{l+2})$ which are given in terms of a local coordinate system $\xi$, where $\xi = x - x_l$ and $0 \leqslant \xi \leqslant h$, by

$$\begin{matrix} \phi_{l-1} \\ \phi_l \\ \phi_{l+1} \\ \phi_{l+2} \end{matrix} \quad \frac{1}{h^3} \begin{cases} (h-\xi)^3 \\ h^3 + 3h^2(h-\xi) + 3h(h-\xi)^2 - 3(h-\xi)^3 \\ h^3 + 3h^2\xi + 3h\xi^2 - 3\xi^3 \\ \xi^3, \qquad 0 \leqslant \xi \leqslant h. \end{cases} \tag{5}$$

All other splines are zero over this element. The variation of $U(x, t)$ over the element is given by

$$U(x, t) = \sum_{j=l-1}^{l+2} c_j \phi_j(x), \qquad [x_l, x_{l+1}]. \tag{6}$$

The $\phi_j(x)$, which are graphed in Fig. 1, thus act as shape functions for the element, with the $c_j$ as element parameters. It is this form for the cubic $B$-splines, showing the variation of all contributing splines over a single interval, which is most useful in the finite element approach rather than the more usual expression showing the variation of a single spline over several intervals. The nodal values of $U(x, t)$ and the derivatives at the nodes are given in terms of the element parameters by

$$\begin{aligned} U_l &= U(x_l) = c_{l-1} + 4c_l + c_{l+1} \\ U_l' &= U'(x_l) = \frac{3}{h}(c_{l+1} - c_{l-1}) \\ U_l'' &= U''(x_l) = \frac{6}{h^2}(c_{l+1} - 2c_l + c_{l-1}), \end{aligned} \tag{7}$$

where the symbol $'$ denotes differentiation with respect to $x$.

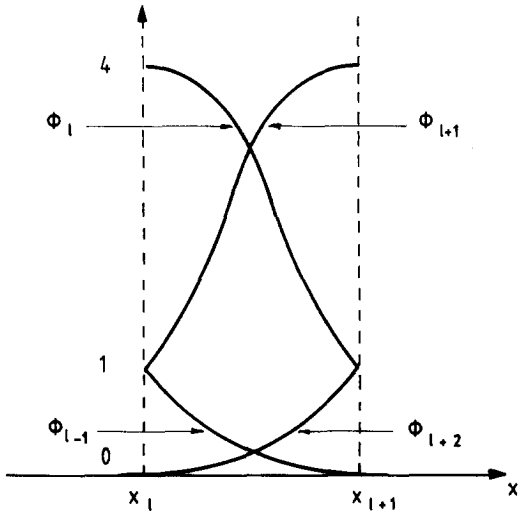


FIG. 1. The cubic $B$-splines covering the element $[x_l, x_{l+1}]$.

The finite element equations that we shall set up will not be expressed in terms of the four nodal parameters $U_l$, $U_l^{|}$ as is the case with cubic Hermite interpolation functions, but in terms of the four element parameters $c_l$, so that we shall not directly determine the nodal values as is the case with the usual finite element formulations [9]. However, these can always be recovered, when required, using Eq. (7).

For a typical element we have the contribution

$$\int_{x_l}^{x_{l+1}} [W(U_t + UU_x) + \delta W_x U_{xt}]\, dx. \tag{8}$$

Now using (7) in (8) and identifying the weight function $W(x)$ with a cubic spline we obtain

$$\begin{aligned} &\sum_{j=l-1}^{l+2} \left[\int_{x_l}^{x_{l+1}} \phi_i \phi_j \, dx\right] \mathring{c}_j^e \\ &\quad + \delta \sum_{j=l-1}^{l+2} \left[\int_{x_l}^{x_{l+1}} \phi_i^{|} \phi_j^{|} \, dx\right] \mathring{c}_j^e \\ &\quad + \sum_{j=l-1}^{l+2} \sum_{k=l-1}^{l+2} \left[\int_{x_l}^{x_{l+1}} \phi_i \phi_j^{|} \phi_k \, dx\right] c_k c_j, \end{aligned} \tag{9}$$

which can be written in matrix form as

$$[\mathbf{A}^e + \delta \mathbf{D}^e]\, \mathring{\mathbf{c}}^e + \mathbf{c}^{eT} \mathbf{L}^e \mathbf{c}^e, \tag{10}$$

where

$$\mathbf{c}^e = (c_{l-1}, c_l, c_{l+1}, c_{l+2})^T. \tag{11}$$

The element matrices are given by the integrals

$$\mathbf{A}^e_{ij} = \int_{x_l}^{x_{l+1}} \phi_i \phi_j \, dx \tag{12}$$

$$\mathbf{D}^e_{ij} = \int_{x_l}^{x_{l+1}} \phi_i^{|} \phi_j^{|} \, dx \tag{13}$$

and

$$\mathbf{L}^e_{ijk} = \int_{x_l}^{x_{l+1}} \phi_i \phi_j^{|} \phi_k \, dx, \tag{14}$$

where $i, j, k$ take only the values $l-1$, $l$, $l+1$, $l+2$ for the typical element $[x_l, x_{l+1}]$. The matrices $\mathbf{A}^e$ and $\mathbf{D}^e$ are therefore $4\times 4$ and $\mathbf{L}^e$ is $4\times 4\times 4$. An associated $4\times 4$ matrix

$$\mathbf{B}^e_{ij} = \sum_{k=l-1}^{l+2} \mathbf{L}^e_{ijk} c^e_k \tag{15}$$

which depends also upon the parameters $c^e_k$ is used in the following theoretical discussions. The element matrices $\mathbf{A}^e$, $\mathbf{D}^e$, $\mathbf{L}^e$, and $\mathbf{B}^e$ were determined algebraically from Eq. (5) using REDUCE [8]. We obtain

$$\mathbf{A}^e = \frac{h}{140}\begin{pmatrix} 20 & 129 & 60 & 1 \\ 129 & 1188 & 933 & 60 \\ 60 & 933 & 1188 & 129 \\ 1 & 60 & 129 & 20 \end{pmatrix} \tag{16}$$

$$\mathbf{D}^e = \frac{1}{10h}\begin{pmatrix} 18 & 21 & -36 & -3 \\ 21 & 102 & -87 & -36 \\ -36 & -87 & 102 & 21 \\ -3 & -36 & 21 & 18 \end{pmatrix} \tag{17}$$

and

$$B^e_{11} = -\tfrac{1}{840}(280, 1605, 630, 5)\,\mathbf{c}^e$$

$$B^e_{12} = -\tfrac{1}{840}(150, 1305, 792, 21)\,\mathbf{c}^e$$

$$B^e_{13} = \tfrac{1}{840}(420, 2781, 1314, 21)\,\mathbf{c}^e$$

$$B^e_{14} = \tfrac{1}{840}(10, 129, 108, 5)\,\mathbf{c}^e$$

$$B^e_{21} = -\tfrac{1}{840}(1605, 10830, 5349, 108)\,\mathbf{c}^e$$

$$B^e_{22} = -\tfrac{1}{840}(1305, 17640, 17541, 1314)\,\mathbf{c}^e$$

$$B^e_{23} = \tfrac{1}{840}(2781, 25002, 17541, 792)\,\mathbf{c}^e$$

$$B^e_{24} = \tfrac{1}{840}(129, 3468, 5349, 630)\,\mathbf{c}^e$$

$$B^e_{31} = -\tfrac{1}{840}(630, 5349, 3468, 129)\,\mathbf{c}^e$$

$$B^e_{32} = -\tfrac{1}{840}(792, 17541, 25002, 2781)\,\mathbf{c}^e$$

$$B^e_{33} = \tfrac{1}{840}(1314, 17541, 17640, 1305)\,\mathbf{c}^e$$

$$B^e_{34} = \tfrac{1}{840}(108, 5349, 10830, 1605)\,\mathbf{c}^e$$

$$B^e_{41} = -\tfrac{1}{840}(5, 108, 129, 10)\,\mathbf{c}^e$$

$$B^e_{42} = -\tfrac{1}{840}(21, 1314, 2781, 420)\,\mathbf{c}^e$$

$$B^e_{43} = \tfrac{1}{840}(21, 792, 1305, 150)\,\mathbf{c}^e$$

$$B^e_{44} = \tfrac{1}{840}(5, 630, 1605, 280)\,\mathbf{c}^e,$$

where $\mathbf{c}^e$ is given by Eq. (11).

Assembling contributions from all elements leads to the equation

$$(\mathbf{A} + \delta\mathbf{D})\,\dot{\mathbf{c}} + \mathbf{B}\mathbf{c} = 0, \tag{18}$$

where

$$\mathbf{c} = (c_{-1}, c_0, c_1, \ldots, c_{N+1})^{\mathrm{T}}, \tag{19}$$

and **A**, **B**, **D** are derived from the element matrices $\mathbf{A}^e$, $\mathbf{B}^e$, $\mathbf{D}^e$ in the usual way. The three assembled matrices are septadiagonal. The general row for each matrix has the following form.

$$\mathbf{A}: \frac{h}{140}(1, 120, 1191, 2416, 1191, 120, 1)$$

$$\mathbf{D}: -\frac{1}{10h}(3, 72, 45, -240, 45, 72, 3)$$

$$\mathbf{B}: \frac{1}{840}(-(5, 108, 129, 10, 0, 0, 0)\,\mathbf{c}, -(21, 1944, 8130, 3888, 129, 0, 0)\,\mathbf{c},$$
$$-(-21, 0, 17841, 35682, 8130, 108, 0)\,\mathbf{c},$$
$$(5, 1944, 17841, 0, -17841, -1944, -5)\,\mathbf{c},$$
$$(0, 108, 8130, 35682, 17841, 0, -21)\,\mathbf{c}, (0, 0, 129, 3888, 8130, 1944, 21)\,\mathbf{c},$$
$$(0, 0, 0, 10, 129, 108, 5)\,\mathbf{c}),$$

where $\mathbf{c} = (c_{l-3}, c_{l-2}, c_{l-1}, c_l, c_{l+1}, c_{l+2}, c_{l+3})$, for row $l$. The matrices **A** and **D** are symmetric while the form of **B** has a somewhat more complex structure.

We time centre on $t = (n + \frac{1}{2})\Delta_t$ and write

$$\mathbf{c} = \frac{1}{2}(\mathbf{c}^n + \mathbf{c}^{n+1}); \qquad \mathring{\mathbf{c}} = \frac{1}{\Delta_t}(\mathbf{c}^{n+1} - \mathbf{c}^n), \tag{20}$$

where $\mathbf{c}^n$ are the parameters at time level $n\Delta_t$ and $\Delta_t$ is the timestep. Equation (18) can now be written

$$\left[\mathbf{A} + \delta\mathbf{D} + \frac{\Delta_t}{2}\mathbf{B}\right]\mathbf{c}^{n+1} = \left[\mathbf{A} + \delta\mathbf{D} - \frac{\Delta_t}{2}\mathbf{B}\right]\mathbf{c}^n, \tag{21}$$

which is a recurrence relationship for the temporal development of **c**. In Eq. (21), **B** depends on $\mathbf{c} = \frac{1}{2}(\mathbf{c}^n + \mathbf{c}^{n+1})$. The following general solution procedure is therefore adopted.

1. Approximate **B** by **B*** derived from $\mathbf{c}^* = \mathbf{c}^n + \frac{1}{2}(\mathbf{c}^n - \mathbf{c}^{n-1})$, and obtain a first approximation to $\mathbf{c}^{n+1}$ from Eq. (21).

2. Iterate two or three times to refine the approximation to $\mathbf{c}^{n+1}$.

Now proceed to the next time step, and repeat this procedure.

For the initial step we approximate **B** by **B*** calculated from $\mathbf{c}^0$ only. The approximation to $\mathbf{c}^1$ is refined by iterating up to 10 times.

From **c** using Eqs. (6) and (7) the time dependence of the solution $U(x, t)$ can be determined. Equations (21) are septadiagonal in form and can be easily and directly solved. To start the process an initial vector $\mathbf{c}^0$ must be determined from the conditions $U(x, 0)$; this is discussed in Section 5.

## 4. Linear Stability Analysis of the Numerical Scheme

The von Neumann stability theory is applied and the growth of a Fourier mode

$$c_j^n = \hat{c}^n e^{ikjh}, \tag{22}$$

where $k$ is the mode number and $h$ is the element size, is determined for a linearisation of the numerical scheme (21).

In this linearisation we assume that the quantity $U$ in the nonlinear term $UU_x$ is locally constant. This is equivalent to assuming that the corresponding values of $c_j$ are also constant and equal to $c$.

Substituting the Fourier mode (22) into Eq. (21) we obtain

$$\hat{c}^{n+1} = g\hat{c}^n, \tag{23}$$

where the growth factor $g$ has the form

$$g = \frac{a - ib}{a + ib}. \tag{24}$$

with

$$a = 2(P - 3Q)\cos 3kh + 2(120P - 72Q)\cos 2kh + (1191P - 45Q)\cos kh + 2416P + 240Q$$

$$b = 6R \sin 3kh + 336R \sin 2kh + 1470R \sin kh$$

and

$$P = \frac{h}{140}, \qquad Q = \frac{\delta}{10h}, \qquad R = \frac{c\Delta_t}{20}.$$

The magnitude of the growth factor is thus

$$|g| = \sqrt{g\bar{g}} = 1, \tag{25}$$

and the linearised scheme is unconditionally stable.

## 5. The Initial State

To determine the initial vector $\mathbf{c}^0$ from the initial condition on $U_N(x, 0)$ we first rewrite Eq. (4) for the initial condition

$$U_N(x, 0) = \sum_{j=-1}^{N+1} c_j^0 \phi_j(x),$$

where we seek the $c_j^0$. To do this we require $U_N(x, 0)$ to satisfy the following constraints:

(a) It shall agree with the initial conditions $U(x, 0)$ at the knots $x_j$, $j = 0, ..., N$.

(b) Periodic boundary conditions will be satisfied, $U(x_0) = U(x_N)$.

This leads to an equation of the form

$$\mathbf{A}\mathbf{c}^0 = \mathbf{b}. \tag{26}$$

This matrix equation is nearly tridiagonal so apply a variant of the Thomas algorithm for its solution.

## 6. The Test Problems

We now validate our algorithm by studying the motion and interaction of solitary waves.

It is well known that Eq. (1) has a two parameter analytic solution of the form

$$U(x, t) = b + 3c \operatorname{sech}^2\{k[x - x_0 - (b + c)t]\}, \tag{27}$$

where

$$k=\frac{1}{2}\sqrt{\frac{c}{\delta(b+c)}}, \tag{28}$$

and $b$ and $c$ are constants.

This solution, with $b=1$, is physically valid and corresponds to that used by Eilbeck and McGuire [3] and Santarelli [11] and applies to a single solitary wave of magnitude $3c$, initially centred on $x_0$, propagating to the right without change of shape at a steady velocity $(1+c)$.

Olver [13] has shown that the RLW equation possesses only three polynomial invariants. We examine the conservation properties of the algorithm by calculating these invariants, which for the RLW equation in the form (1) are

$$C_1=\int_a^b U\,dx,$$

$$C_2=\int_a^b (U^2+\delta U_x^2)\,dx,$$

and

$$C_3=\int_a^b U^3\,dx.$$

First, we consider the motion of a single solitary wave and take as initial condition

$$U(x,0)=1+3c\,\mathrm{sech}^2(Ax+D) \tag{29}$$

with $c=0.3$, $\delta=1.0$, $A=\frac{1}{2}(c/\delta(1+c))^{1/2}$ and $D=-40A$. The range $0\leqslant x\leqslant 80$ is divided into 400 elements of equal length 0.2 and a time step $\Delta t=0.1$ used. We

TABLE I

| Time | $C_1$ | $C_2$ | $C_3$ | $L_2\times 10^3$ |
|---|---|---|---|---|
| 0.0 | 87.4940 | 99.6920 | 119.2087 | 0.018 |
| 0.5 | 87.4941 | 99.6922 | 119.2089 | 0.109 |
| 1.0 | 87.4942 | 99.6923 | 119.2091 | 0.199 |
| 1.5 | 87.4944 | 99.6927 | 119.2095 | 0.289 |
| 2.0 | 87.4945 | 99.6930 | 119.2100 | 0.378 |
| 2.5 | 87.4947 | 99.6943 | 119.2104 | 0.472 |
| 3.0 | 87.4949 | 99.6936 | 119.2110 | 0.565 |
| 3.5 | 87.4951 | 99.6940 | 119.2114 | 0.657 |
| 4.0 | 87.4953 | 99.6943 | 119.2118 | 0.747 |
| 4.5 | 87.4955 | 99.6948 | 119.2125 | 0.832 |
| 5.0 | 87.4957 | 99.6951 | 119.2130 | 0.901 |

observe the solitary wave move to the right unchanged in form and with a velocity $c = 1.3$.

To examine more carefully the behaviour of the numerical scheme we use the $L_2$ norm to compare the numerical with the exact solution (27) and the quantities $C_1$, $C_2$, and $C_3$ to measure conservation. Our results are given in Table I. We see that $C_1$, $C_2$, and $C_3$ are satisfactorily constant, each changing less than $5 \times 10^{-3}\%$ during the experiment. The $L_2$ error is also small compared with values quoted by

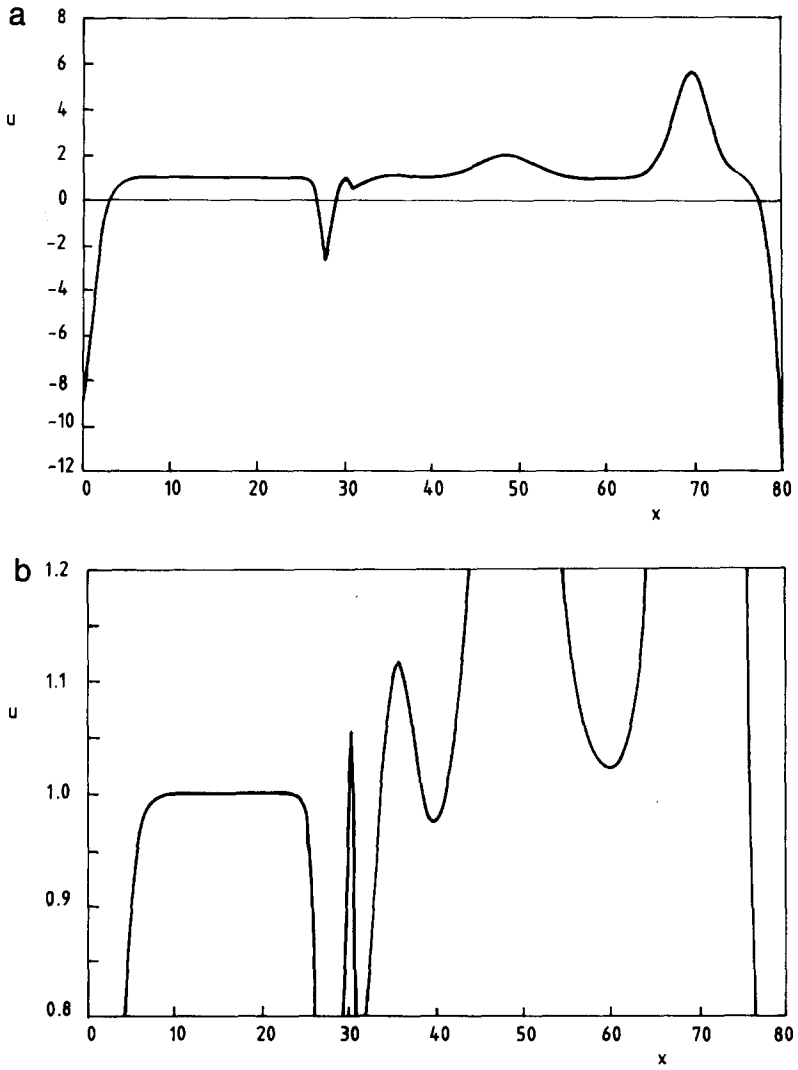


FIG. 2. Santarelli experiment. (a) State at time $t = 20$. (b) As (a) with expanded vertical scale.

other authors [10]. An expansion of the $y$-scale indicates from the solution curve that the error in the numerical method is of order $10^{-6}$.

Santarelli [11] has simulated the interaction of a positive and a negative solitary wave and observed the collision to produce additional solitary waves, an observation confirmed by Courtenay Lewis and Tjon [12]. We have repeated those experiments using the appropriate initial condition

$$U(x, 0) = 1 + U_1 + U_2,$$

where

$$U_j = 3A_j \operatorname{sech}^2[k_j(x - \bar{x}_j - v_j t)],$$

and

$$A_j = \frac{4k_j^2}{1 - 4k_j^2}, \qquad v_j = \frac{1}{1 - 4k_j^2} = 1 + A_j$$

and solved the RLW equation over the region $0 \leqslant x \leqslant 80$ taking $\delta = 1.0$ and $k_1 = 0.4$, $\bar{x}_1 = 23$, $k_2 = 0.6$, $\bar{x}_2 = 38$, $h = 0.2$, and $\Delta t = 0.1$. Our results confirm the observations given in Figs. 1–9 of [11] in all details. In Fig. 2a we show the state at time $t = 20.0$.

The smaller of the original pair of waves now lies at $x = 70$, and the larger (negative) wave is passing through the right-hand end of the region and reappearing at the left-hand end (the boundary conditions are periodic). The interval between $x = 7$ and $x = 23$ is the undisturbed part of the region, away from the pulse, where the solution remains 1. The waves lying between $x = 25$ and $x = 60$ have resulted from the interaction. We have expanded the vertical scale in Fig. 2b to show details of the structure of these waves. The point $x = 30$, where the curves show a sharp maximum, is the site of the original collision. Daughter waves appear to be emanating from this point.

The values of $C_1$, $C_2$, and $C_3$ throughout the simulation are shown in Table II. The quantity $C_1$ in both sets of results is conserved to within $10^{-2}\%$, and in the present simulation $C_2$ changes by less than $5 \times 10^{-2}\%$ and $C_3$ by less than 0.5%.

TABLE II

| Time | $C_1$ | $C_2$ | $C_3$ | $C_1$ [11] |
|---|---|---|---|---|
| 0.0 | 73.9394 | 450.7290 | 289.0589 | −6.060606 |
| 4.0 | 73.9545 | 449.3988 | 286.0132 | −6.060603 |
| 8.0 | 73.9431 | 450.5612 | 288.7828 | −6.060552 |
| 12. | 73.9496 | 450.6183 | 288.2262 | −6.060179 |
| 14. | 73.9522 | 450.5971 | 288.0318 | −6.059980 |
| 16. | 73.9550 | 450.5750 | 287.8357 | |
| 20. | 73.9604 | 450.5330 | 287.4558 | |

Abdulloev *et al.* [2] have studied the interaction of two positive solitary waves and observed an almost stationary rarefaction wave of small amplitude ($\sim 10^{-3}$) with an exceedingly low velocity ($< 3 \times 10^{-5}$) left behind the two diverging solitary waves of magnitudes about 6 and 2. We have chosen to study a similar situation using as initial condition

$$U(x, 0) = 1 + U_1 + U_2,$$

where

$$U_j = 3A_j \operatorname{sech}^2[k_j(x - \bar{x}_j)],$$

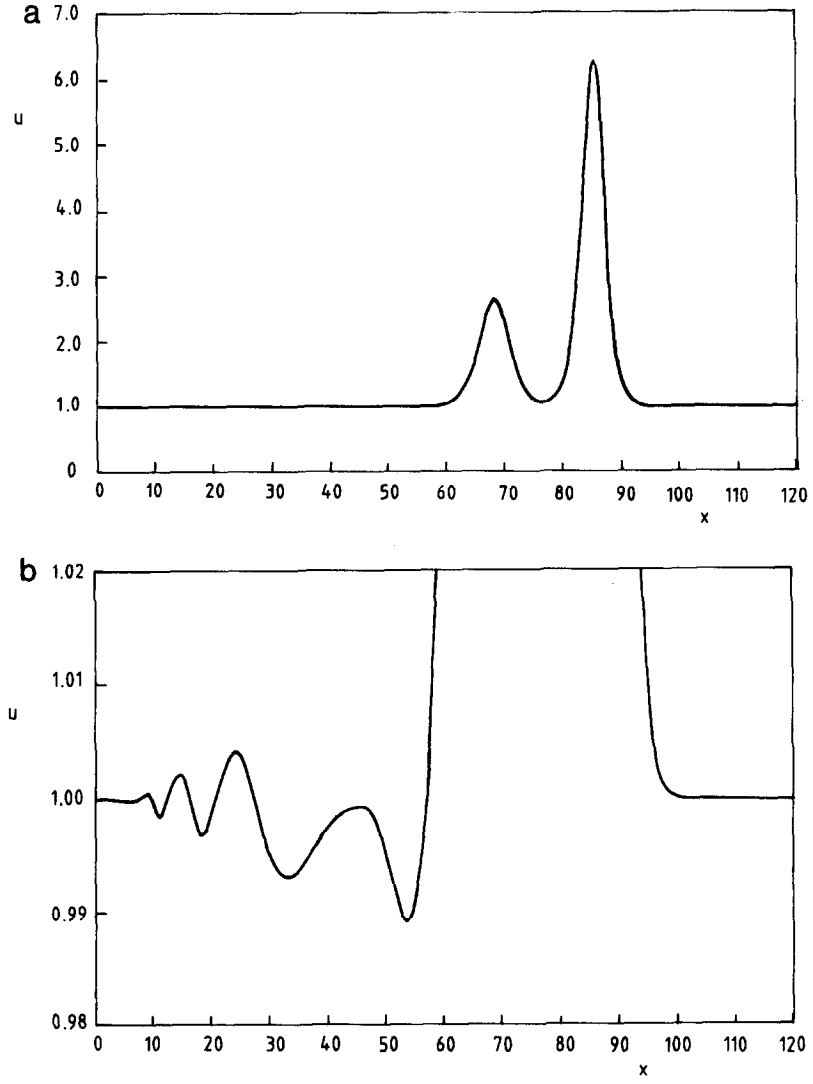


FIG. 3. Abdulloev experiment. (a) State at time $t = 25$. (b) As (a) with expanded vertical scale.

and

$$A_j = \frac{4k_j^2}{1-4k_j^2}.$$

The RLW equation was solved over the region $0 \leqslant x \leqslant 120$ taking $\delta = 1.0$ and $k_1 = 0.4$, $\bar{x}_1 = 15$, $k_2 = 0.3$, $\bar{x}_2 = 35$, $h = 0.3$, and $\Delta_t = 0.1$.

The configuration at time $t = 25$, which is some time after the interaction is complete, is shown in Fig. 3a. The two waves have apparently passed through one

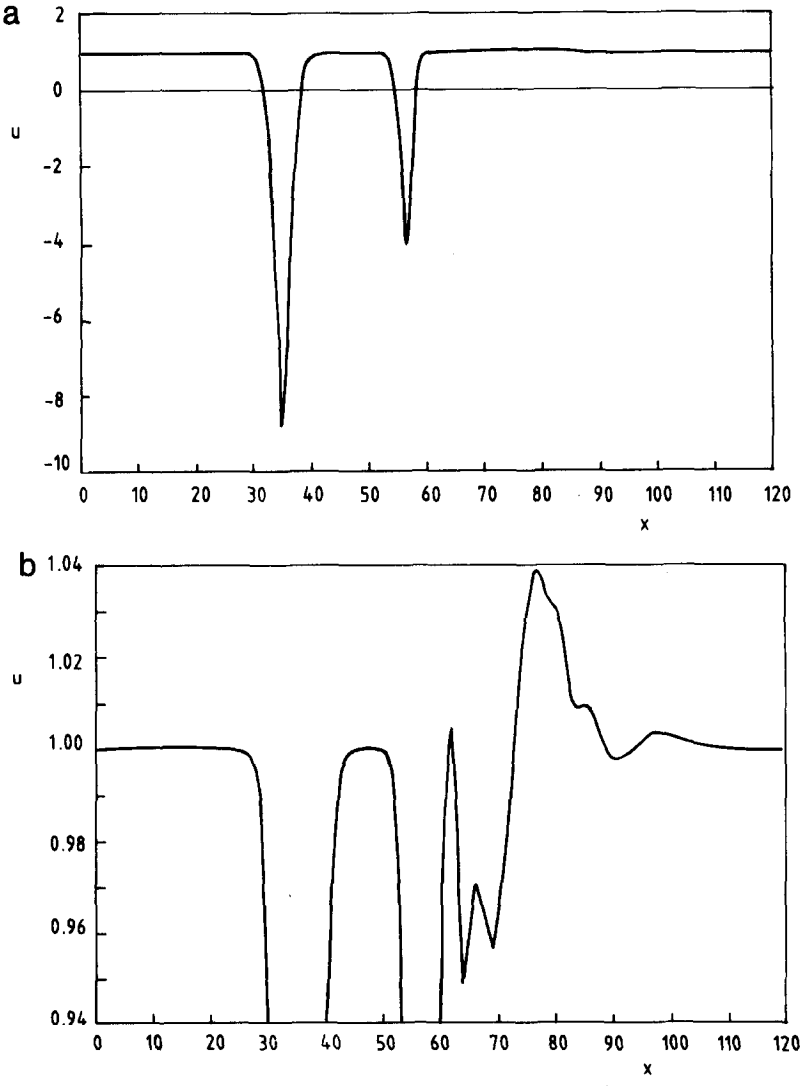


FIG. 4. Interaction of two negative waves. (a) State at time = 20. (b) As (a) with expanded vertical scale.

TABLE III

| Time | $C_1$ | $C_2$ | $C_3$ |
|---|---|---|---|
| 0 | 157.916 | 316.355 | 977.83 |
| 4 | 157.914 | 316.350 | 977.81 |
| 8 | 157.913 | 316.348 | 977.76 |
| 12 | 157.912 | 316.344 | 977.34 |
| 16 | 157.911 | 316.342 | 977.42 |
| 20 | 157.910 | 316.340 | 977.74 |
| 24 | 157.910 | 316.336 | 977.75 |
| 27 | 157.909 | 316.335 | 977.75 |
| 30 | 157.908 | 316.332 | 977.74. |

another and emerged unchanged by the encounter. Under magnification, Fig. 3b, we observe an oscillation of small amplitude, average $\sim 5 \times 10^{-3}$, trailing behind the solitary waves. This is in accord with the observations of Abdulloev *et al.* [2].

In Table III we record the values of the invariants $C_1$, $C_2$, and $C_3$ for times throughout the simulation. We see that each is satisfactorily conserved, as each changes by less than $10^{-2}\%$ during the computer run.

In addition we have studied the interaction of two negative solitary waves over the region $0 \leqslant x \leqslant 120$ using the previous initial condition with $\delta = 1$, $k_1 = 0.6$, $\bar{x}_1 = 82$, $k_2 = 0.8$, $\bar{x}_2 = 67$, $h = 0.3$, and $\Delta_t = 0.1$.

After the interaction is completed we have the situation shown in Fig. 4a. The two waves have changed little but there is some evidence of an additional distur-

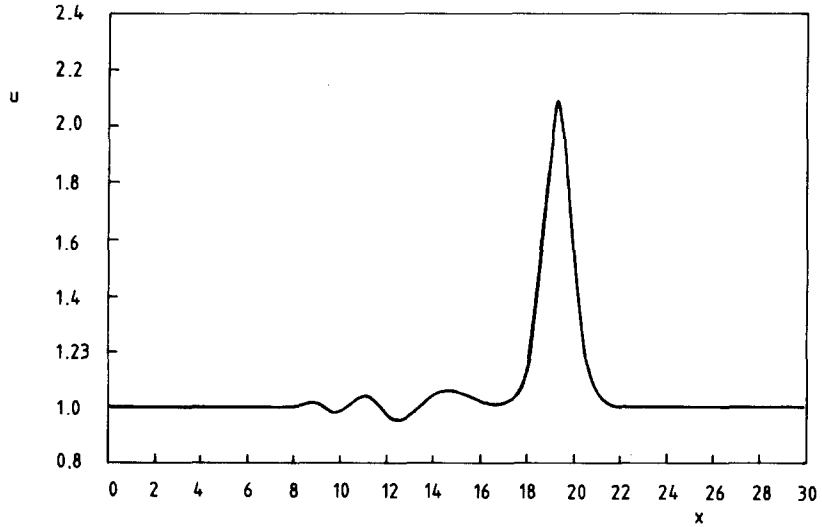


FIG. 5. Maxwellian initial condition $\delta = 0.04$. State at $t = 9$.

TABLE IV

| Time | $C_1$ | $C_2$ | $C_3$ |
|---|---|---|---|
| 0 | 74.97 | 366.89 | 1092.9 |
| 4 | 74.97 | 366.82 | 1092.4 |
| 8 | 74.97 | 366.78 | 1090.3 |
| 12 | 74.98 | 366.72 | 1091.5 |
| 16 | 74.99 | 366.65 | 1091.0 |
| 20 | 74.99 | 366.59 | 1090.4 |

TABLE V

$\delta = 0.04$

| Time | $C_1$ | $C_2$ | $C_3$ |
|---|---|---|---|
| 0.0 | 31.7725 | 34.8484 | 40.1006 |
| 2.0 | 31.7730 | 34.8492 | 40.1019 |
| 4.0 | 31.7733 | 34.8501 | 40.1029 |
| 6.0 | 31.7737 | 34.8507 | 40.1037 |
| 8.0 | 31.7739 | 34.8509 | 40.1039 |

TABLE VI

$\delta = 0.01$

| Time | $C_1$ | $C_2$ | $C_3$ |
|---|---|---|---|
| 0.0 | 31.7725 | 34.8108 | 40.1006 |
| 2.0 | 31.7725 | 34.8108 | 40.1010 |
| 4.0 | 31.7724 | 34.8106 | 40.1011 |
| 6.0 | 31.7721 | 34.8102 | 40.1006 |
| 8.0 | 31.7719 | 34.8097 | 40.1000 |
| 10. | 31.7718 | 34.8095 | 40.0996 |
| 12. | 31.7718 | 34.8094 | 40.0994 |
| 14. | 31.7718 | 34.8094 | 40.0995 |

TABLE VII

$\delta = 0.001$

| Time | $C_1$ | $C_2$ | $C_3$ |
|---|---|---|---|
| 0.0 | 31.7725 | 34.8016 | 40.1426 |
| 4.0 | 31.7724 | 34.8016 | 40.1426 |
| 8.0 | 31.7724 | 34.8017 | 40.1439 |
| 12. | 31.7724 | 34.8016 | 40.1423 |
| 16. | 31.7724 | 34.8016 | 40.1469 |
| 20. | 31.7725 | 34.8017 | 40.1504 |
| 24. | 31.7725 | 34.8018 | 40.1477 |

bance. Under magnification, Fig. 4b, we see that an oscillation of amplitude $\sim 4 \times 10^{-2}$ is trailing behind the solitary waves.

The values taken by the invariants $C_1$, $C_2$, and $C_3$ over the period of the simulation are given in Table IV. All are satisfactorily conserved; $C_1$ changes by less than $3 \times 10^{-2}\%$, $C_2$ by less than $8 \times 10^{-2}\%$, and $C_3$ by less than 0.25%. These values are of the same order as those found for the Santarelli experiment.

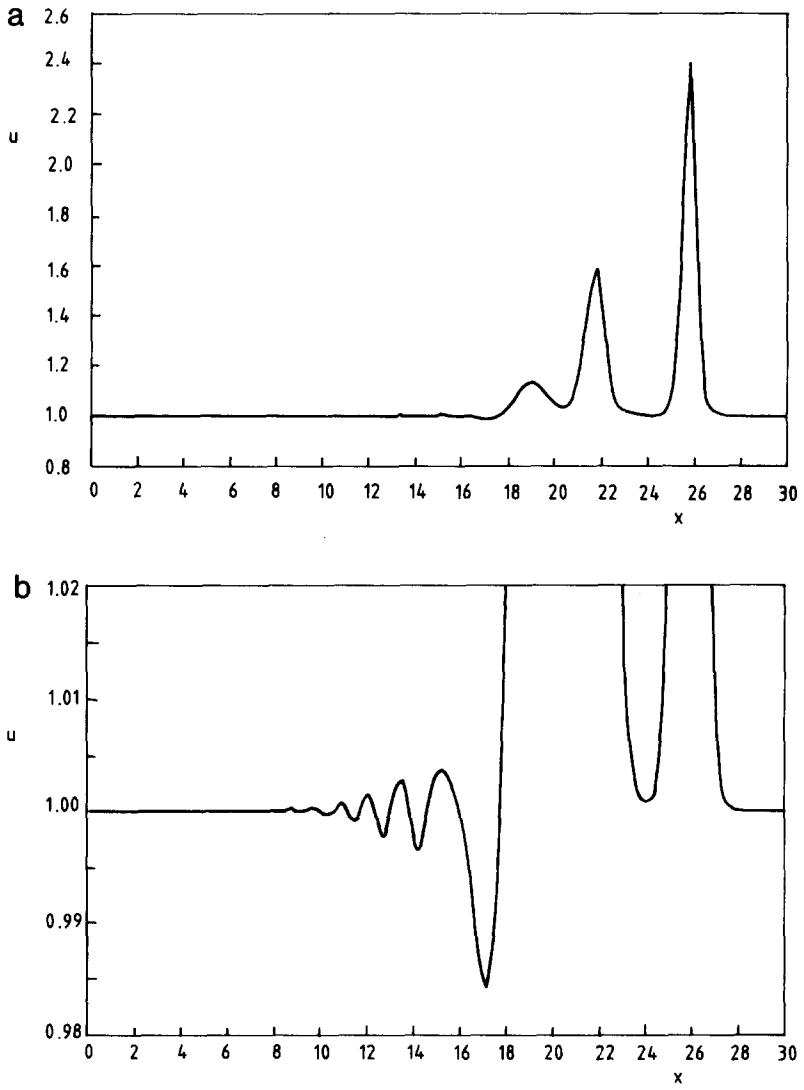


FIG. 6. Maxwellian initial condition $\delta = 0.01$. (a) State at time $t = 17$. (b) As (a) with expanded vertical scale.

Finally, we have examined, for various values of the parameter $\delta$, the evolution of an initial Maxwellian pulse into solitary waves, using as initial condition

$$U(x, 0) = 1 + \exp(-(x-7)^2).$$

For $\delta = 0.04$ the Maxwellian develops into a single solitary wave with magnitude and velocity consistent with Eq. (27), plus a well developed oscillating tail as shown in Fig. 5. This result bears a strong resemblance to the corresponding KdV simulation. The values of the quantities $C_1$, $C_2$, and $C_3$ are given in Table V; each is satisfactorily constant as the maximum change is less than 0.01 %.

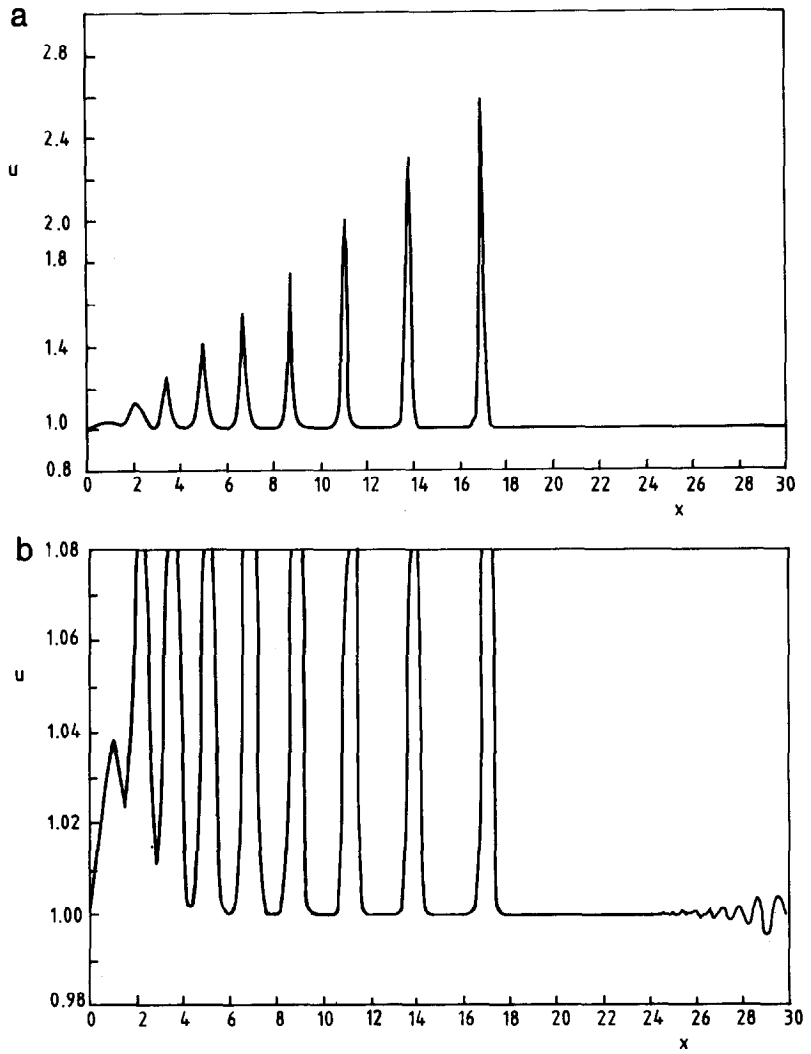


FIG. 7. Maxwellian initial condition $\delta = 0.001$. (a) State at $t = 25$. (b) As (a) with expanded vertical scale. Periodic boundary conditions.

When $\delta$ has a value of 0.01 the final state is composed of three solitary waves, Fig. 6a, each of which has magnitude and velocity consistent with Eq. (27). The breakup into solitary waves is not clean however as a small disturbance is evident behind the wave. When the vertical scale is magnified as in Fig. 6b it is seen clearly to be an oscillation of magnitude $\sim 10^{-2}$. The values of the invariants $C_1$, $C_2$, and $C_3$ are given in Table VI. These each change by less than 0.005% during the run.

With $\delta = 0.001$ the final state is made up from nine solitary waves, Figure 7a, whose peaks lie on a straight line so that their velocities are linearly dependent on their amplitudes and in fact obey a relationship consistent with Eq. (27). On magnification of the $y$-scale a well developed oscillating tail is again evident trailing behind the train of solitary waves; the tail appears at the right of Fig. 7b, and periodic boundary conditions are used. It thus appears that the initial Maxwellian pulse breaks up into a train of solitary waves, the number depending on the value of $\delta$; however, the breakup is not clean and on magnification of the vertical scale we have always observed a small oscillating tail. The invariants for this problem are listed in Table VII. Observed changes are each less than 0.001%.

The critical value of $\delta$ for the KdV equation is $\delta = 0.0625$ [14], for which value the nonlinear and dispersive terms balance and the initial pulse travels across the mesh unchanged in form. In the RLW case a small oscillation of magnitude about $2 \times 10^{-2}$ is again observed behind the pulse. There is, of course, no reason to suppose that the critical values for these two equations should exactly coincide.

For values of $\delta$ greater than the critical value solitary waves are not expected [14]. We have set up a simulation for $\delta = 1$ and find that the solution is a rapidly oscillating wave packet similar to those observed for the KdV equation.

## 7. Conclusions

We have shown that the finite element method set up in Section 3 can faithfully represent the amplitude, position, and velocity of a single solitary wave and that the interactions of two solitary waves as described by Abdulloev *et al.* [2] and Santarelli [11] are satisfactorily reproduced. The small stationary wave observed by Abdulloev *et al.* is confirmed in our simulation and the figures given by Santarelli agree in all particulars with those reproduced in Section 6 and show the generation of large amplitude (up to 4) daughter waves. The three invariants of motion are satisfactorily constant in all the computer simulations described here, so that the algorithm can fairly be described as conservative. The numerical scheme has been shown to be unconditionally stable and a run on a VAX 8650 using 150 nodes and 100 time steps took 2.5 s of CPU time, so the scheme is reasonably efficient. We have further shown that the algorithm copes well with the generation of solitary waves from an arbitrary initial pulse and conclude that it may with confidence be used for runs of the RLW equation which are of long duration.

We have demonstrated that, if used in the way described in Section 3, cubic

splines are as easy to apply as element shape functions as are the ubiquitious linear polynomials. We believe that this approach will be useful also for other applications where continuity of derivatives is essential.

## ACKNOWLEDGMENTS

We thank the referees for several useful suggestions, especially that the final problem studied in Section 6 should be included.

## REFERENCES

1. D. H. PEREGRINE, *J. Fluid. Mech.* **25**, 321 (1966).
2. KH. O. ABDULLOEV, H. BOGOLUBSKY, AND V. G. MARKHANKOV, *Phys. Lett. A* **56**, 427 (1976).
3. J. C. EILBECK AND G. R. MCGUIRE, *J. Comput. Phys.* **23**, 63 (1977).
4. J. L. BONA, W. G. PRITCHARD, AND L. R. SCOTT, *J. Comput. Phys.* **60**, 167 (1985).
5. M. E. ALEXANDER AND J. H. MORRIS, *J. Comput. Phys.* **30**, 428 (1979).
6. L. WAHLBIN, *Numer. Math.* **23**, 289 (1975).
7. P. M. PRENTER, *Splines and Variational Methods* (Wiley, New York, 1975).
8. A. C. HEARN, "REDUCE Users Manual Version 3.2" (Northwest Computer Algorithms, 1986).
9. O. C. ZIENKIEWICZ, *The Finite Element Method*, 3rd ed. (McGraw–Hill, London, 1979).
10. J. M. SANZ SERNA AND I. CHRISTIE, *J. Comput. Phys.* **39**, 94 (1981).
11. A. R. SANTARELLI, *Nuovo Cimento B* **46**, 179 (1978).
12. J. COURTENAY LEWIS AND J. A. TJON, *Phys. Lett. A* **73**, 275 (1979).
13. P. J. OLVER, *Math. Proc. Cambridge Philos. Soc.* **85**, 143 (1979).
14. YU. A. BEREZIN AND V. I. KARPMAN, *Sov. Phys. JEPT* **24**, 1049 (1967).